Evolution of dispersoids and their effects on elevated-temperature strength and creep resistance in Al-Si-Cu 319 cast alloys with Mn and Mo additions

Lanfeng Jin, Kun Liu, X.-Grant Chen *

Department of Applied Sciences, University of Quebec at Chicoutimi
Saguenay, QC, G7H 2B1, Canada
(*Corresponding author: xgrant_chen@uqac.ca; Tel.: 1-418 5455011 ext. 2603)

Abstract

The present work investigated the evolution of dispersoids during various heat treatments via Mn and Mo additions and studied their effects on the yield strength (YS) and creep resistance at elevated temperature in Al-Si-Cu 319 cast alloys. The results showed that the individual addition of Mn or Mo promoted the precipitation of α-dispersoids; however, the best effect was achieved by their combined addition. The optimum heat treatment condition was at 500°C for 8 h; under this condition, the largest quantity of and the finest α-dispersoids were obtained, resulting in remarkable improvements in YS at both room and elevated temperatures. The creep resistance at 300°C was enhanced owing to the additions of Mn and Mo. Compared with the properties of the base alloy, a 19% improvement in YS at 300°C, doubling of threshold stress and a 50-fold reduction in the minimum creep rate on the creep property at 300°C were achieved by the combined addition of Mn and Mo. The alloy with both Mn and Mo exhibited the lowest YS decline rate and no change in the minimum creep rate during prolonged thermal exposure at 300°C for up to 1000 h, demonstrating the superior thermal stability achieved by the 319 alloys with the introduction of a sufficient number of dispersoids from Mn and Mo additions.

Keywords: Al-Si-Cu 319 alloy; elevated-temperature strength; creep resistance; thermal stability

1. Introduction

Heat-treatable Al-Si-Cu cast alloys have been widely used in the automotive and aerospace industries for the fabrication of engine blocks and cylinder heads because of their good castability and high strength-to-weight ratio [1-3]. When the components are in service, the working temperature can reach elevated values (250–350°C). However, the nano-scale precipitates formed by age-hardening treatments (T6/T7) can be rapidly coarsened at elevated temperatures, leading to a sharp decline in the mechanical properties [1]. For instance, the yield strength (YS) of Al-Si 356 under the T7 condition dropped sharply from 165 MPa at room temperature (RT) to 45 MPa at 315°C and further to 24 MPa after serving 1000 h of service at 315°C because of the metallurgical instability of the age-hardening precipitates [4]. Therefore, improving the elevated-temperature

properties of Al-Si(-Cu) cast alloys in automobile and aerospace applications has been one of the vital industrial concerns.

Recently, dispersoid strengthening has been proven to be one of the most practical methods for enhancing the elevated-temperature properties in wrought Al alloys, such as Al-Mn-Mg 3xxx alloys [5-12]. It is reported that the YS at 300°C of the Al-Mn-Mg 3004 alloy increases from 55 MPa to 97 MPa owing to the precipitation of high-volume, fine dispersoids [9-11]. Meanwhile, this type of dispersoids are partially coherent with the Al matrix and are proven to be thermally stable at 300–350°C, leading to superior stability of the elevated-temperature mechanical properties of the 3004 alloy [8, 11]. On the other hand, limited research has been conducted on the strengthening of dispersoids in Al-Si cast alloys. Farkoosh *et al.* [13, 14] found that dispersoids in Al-Si 356 cast alloys can form when solution treated at 540°C, leading to the improved YS and enhanced creep resistance at 300°C. However, the evolution of dispersoids with temperature during heat treatment has not been systematically studied to obtain the optimum conditions of dispersoid precipitation. Furthermore, the evolution of dispersoids and properties during long service durations at elevated temperature has never been reported although these are among the most significant considerations for the safety design of cast components serving at elevated temperature. Therefore, it is significant to explore the potential of Al-Si(-Cu) cast alloys for application at elevated temperature via dispersoid strengthening.

In the present work, two most often added elements, Mn and Mo, as dispersoid former in wrought Al alloys, were introduced into Al-Si-Cu 319 cast alloys to investigate the evolution of dispersoids as well as the elevated-temperature properties. Various heat treatments across a wide range of temperatures (400–500°C) and durations (up to 72 h) were performed to systematically investigate the precipitation behavior of dispersoids. Meanwhile, the YS and creep resistance as well as their evolution during long-term service (up to 1000 h) at 300°C were evaluated with the objective of developing new heat-resistant Al-Si-Cu 319 cast alloys.

2. Experimental

Four Al-Si-Cu 319-type alloys with different Mo and Mn contents were designed in the present work. Alloy A was the base alloy free of Mn and Mo, while Alloys B and C were prepared by individually adding Mn or Mo, respectively, and Alloy D was prepared by the combined addition of the two elements. The chemical compositions of the four alloys, as analyzed by optical emission spectroscopy, are presented in Table 1. According to our previous works [11, 13, 14], the maximum addition of Mn or Mo are limited to 0.3% to avoid the sludge Fe-rich intermetallics or primary Al-Mo particles during solidification. The alloys were prepared in an electric resistance furnace. The temperature of the melt was maintained at 750°C for 30 min and this was followed by degassing for 15 min with pure Ar. The melt was poured into a permanent mold preheated at 250°C to obtain the cast ingots with a dimension of 30 mm × 40 mm × 80 mm.

Table 1 Chemical compositions of the experimental alloys (wt. %).

Alloy	Si	Cu	Mg	Ti	Fe	Mo	Mn	Al
A(Base)	5.99	3.19	0.08	0.10	0.28	**0**	**0**	Bal.
B	6.03	3.42	0.08	0.10	0.22	**0**	**0.24**	Bal.
C	6.02	3.42	0.09	0.14	0.31	**0.32**	**0**	Bal.
D	6.07	3.45	0.09	0.08	0.32	**0.29**	**0.25**	Bal.

To study the evolution of dispersoids during heat treatment, the ingots were heat-treated at 400°C, 450°C, and 500°C at a heating rate of 5°C/min for various holding times of up to 72 h, followed by water quenching to room temperature. Some samples were selected to be artificially aged at 155°C for 5 h after the solution treatment at 500°C to reach the T6 temper conditions. The electrical conductivity (EC) and Vickers microhardness measurements were conducted at room temperature. The EC values of the polished samples were measured using a Sigmascope SMP10 instrument and the average value of five measurements was recorded under each condition. The microhardness was evaluated using an NG-1000 CCD microhardness test machine with a load of 10 g and dwell time of 20 s for at least 10 measurements.

The compressive tests were conducted at 25°C and 300°C using a Gleeble 3800 thermomechanical simulator unit to evaluate YS. The total strain of the deformed samples was 0.2 at a strain rate of 0.001 s^{-1}. The creep tests were performed at 300°C for 100 h under the compression mode using various loads (25–40 MPa). Each condition was repeated at least thrice. The cylindrical samples for the YS and creep tests were each machined to a length of 15 mm and diameter of 10 mm. Since the elevated-temperature properties of experimental alloys were all measured at 300 °C, “ET” was simply used in the following part to indicate the elevated temperature of 300 °C.

To analyze the microstructure evolution, optical microscopy (OM) was performed to characterize the microstructures and verify the distributions of the dispersoid zone and dispersoid free zone (DFZ). To clearly reveal the dispersoids, the polished samples were etched using 0.25% HF for 90 s. Transmission electron microscopy (TEM) operated at 200 kV was conducted to characterize the morphology, size and chemistry of the dispersoids. For the statistical measurements on TEM, at least 10 locations have been observed in 3 TEM foils and at least 200 particles have been analyzed.

3. Results and discussion

3.1 As-cast microstructure

Fig. 1 shows the as-cast microstructures of Alloys A and D, which were composed of Al dendrite cells (Al matrix), eutectic Si particles, θ-Al_2Cu and Fe-rich intermetallics distributed along the dendritic boundaries. The Fe-rich intermetallics in the base alloy (Alloy A) exhibited a plate-like morphology (β-Al_5FeSi), Fig. 1a) and they were

transformed into a Chinese-script-like morphology (α-Al(FeMnMo)Si) in Alloy D (Fig. 1b) owing to the promotion effects of Mn and Mo on the transformation of β-Fe to α-Fe [17]. As the microstructures of the three Mn- and Mo-containing alloys (B, C, and D) are similar, only the typical microstructure of Alloy D is presented. Although a small portion of Mn and Mo combined with the Fe elements to form α-Fe, the majority of Mn or Mo elements remained in the solid solution of the Al matrix in the as-cast condition owing to a relatively low volume of Fe-rich intermetallics (~1.5 vol.%), which is also confirmed by the microhardness and EC values shown in Fig. 1c. The gradual increase in microhardness and decrease in EC from Alloy A to Alloy D indicate the increasing solid solution effect of the Mn or/and Mo contents in Alloys B, C and D.

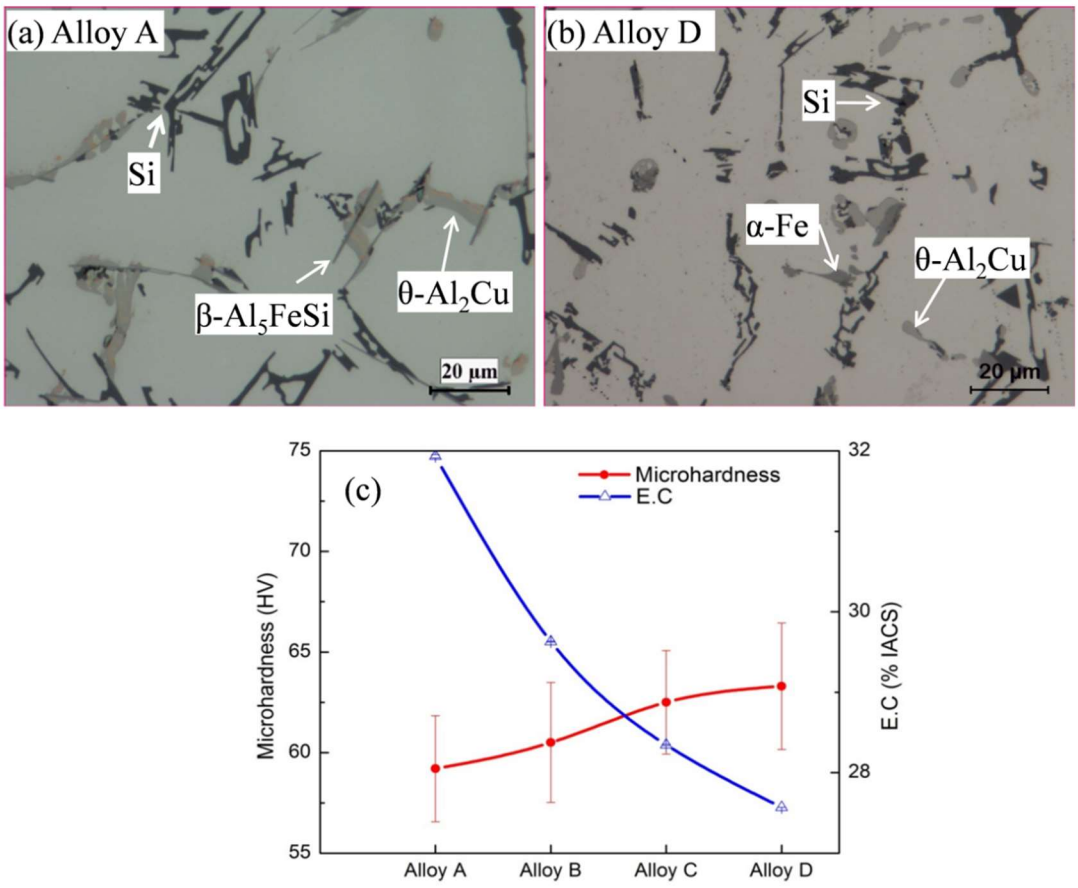

Fig. 1 Typical optical as-cast microstructures of (a) Alloy A, (b) Alloy D, and (c) as-cast microhardness and EC of four alloys

3.2 Evolution of dispersoids during heat treatment

Due to the relatively lower incipient melting temperature of 319 alloys (~520°C) [1], heat treatments up to 500°C for different holding times were performed in the present work to investigate the evolution of dispersoids. The microstructures of Alloys A and D after treatments at 400°C, 450°C, and 500°C for the longest holding time are shown in Fig. 2

for a general observation of the dispersoid appearance.

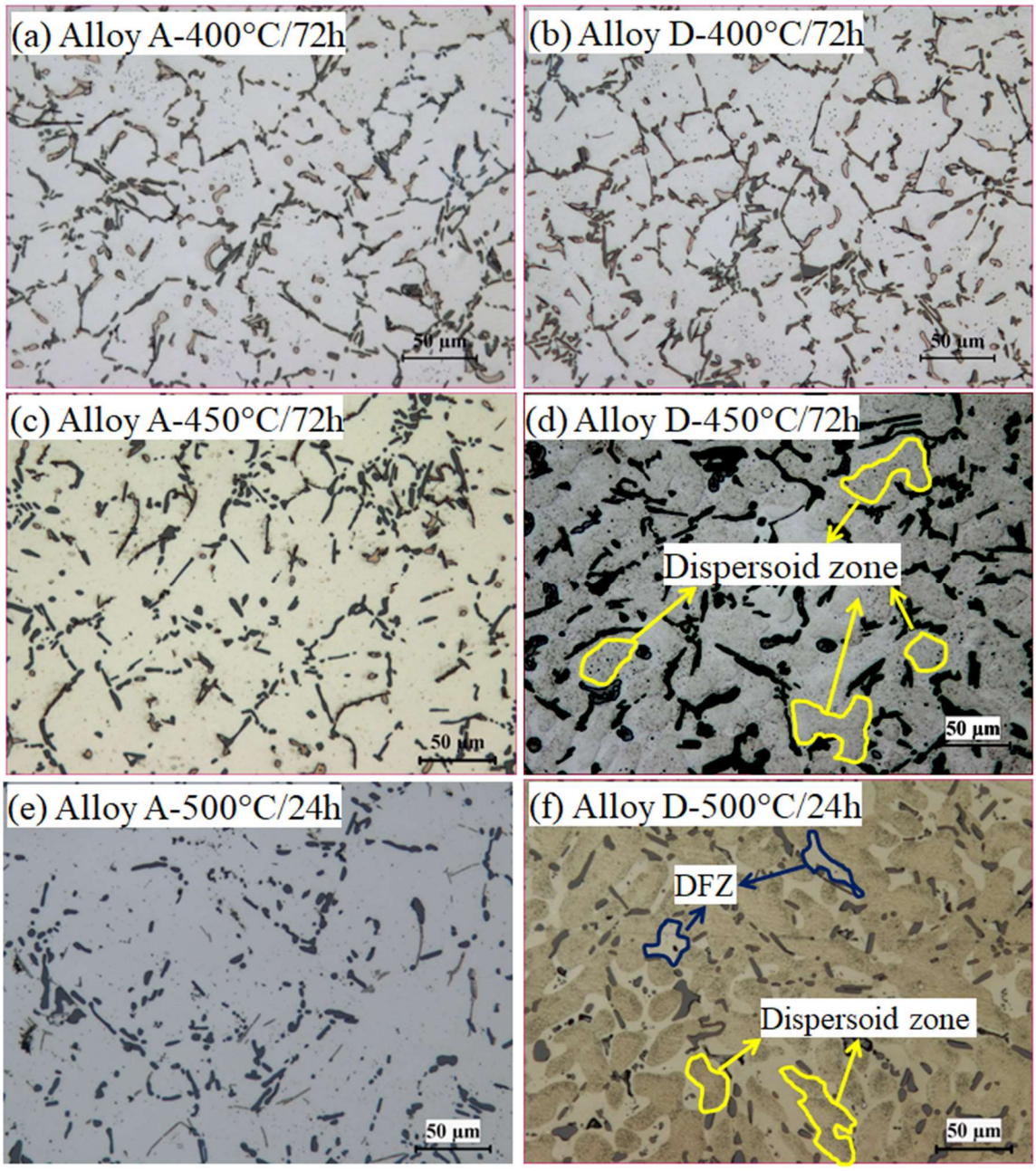

Fig. 2 Optical microstructures heat-treated at various temperatures of Alloys A and D

Apparently, no sign of dispersoids can be observed in Alloy A free of Mn and Mo when treated at 400°C/72h, (Fig. 2a), 450°C/72h (Fig. 2c), and even 500°C/24h (Fig. 2e). In Alloy D, the dispersoids were still absent at 400°C/72h (Fig. 2b) while some very fine dispersoids appeared in the dendrite cells at 450°C/72h (Fig. 2d). With increasing temperature (500°C/24h, Fig. 2f), the formation of dispersoids became obvious as indicated by the clearly distinguished dispersoid zone and DFZ. In addition, the microhardness in

the DFZ is generally lower than that of dispersoids zone due to the contribution of fine dispersoids. For instance, in Alloy D, the microhardness in the DFZ after 450ºC/72h is 73 HV while it is 85 HV in dispersoid zone.

As shown in Fig. 2, the dispersoids started to precipitate after treatment at 450°C/72h and were clearly displayed in the matrix after treatment at 500°C/24h in Alloy D. Since the precipitation of dispersoids was kinetically more favorable at 500°C than 450°C, the following study dominantly focused on the heat treatment at 500°C and the evolution of dispersoids with time in Alloys B, C, and D are presented in Fig. 3. The general tendency was that the dispersoids began to precipitate after 2 h (Figs. 3a–c), increased in volume with time until 8 h (Figs. 3d–f), and then stabilized until 24 h (Figs. 3g–i). The image analysis results of the area percentage of the dispersoid zone in Alloys B, C, and D are shown in Fig. 4, in which the area percentage of the dispersoid zone generally increased from 2 h to 8 h and subsequently formed a plateau until 24 h. Among the three alloys, the area fraction of the dispersoid zone increased in the order, Alloy B < Alloy C < Alloy D, at any given holding time. For instance, after treatment at 500°C/8h, the area percentage of the dispersoid zone in Alloy B reached 53% but increased to 73% in Alloy C and further to 84% in Alloy D respectively, indicating that Mo was more efficient than Mn in promoting the formation of dispersoids but that the combination of Mn and Mo achieved the highest dispersoid zone fraction.

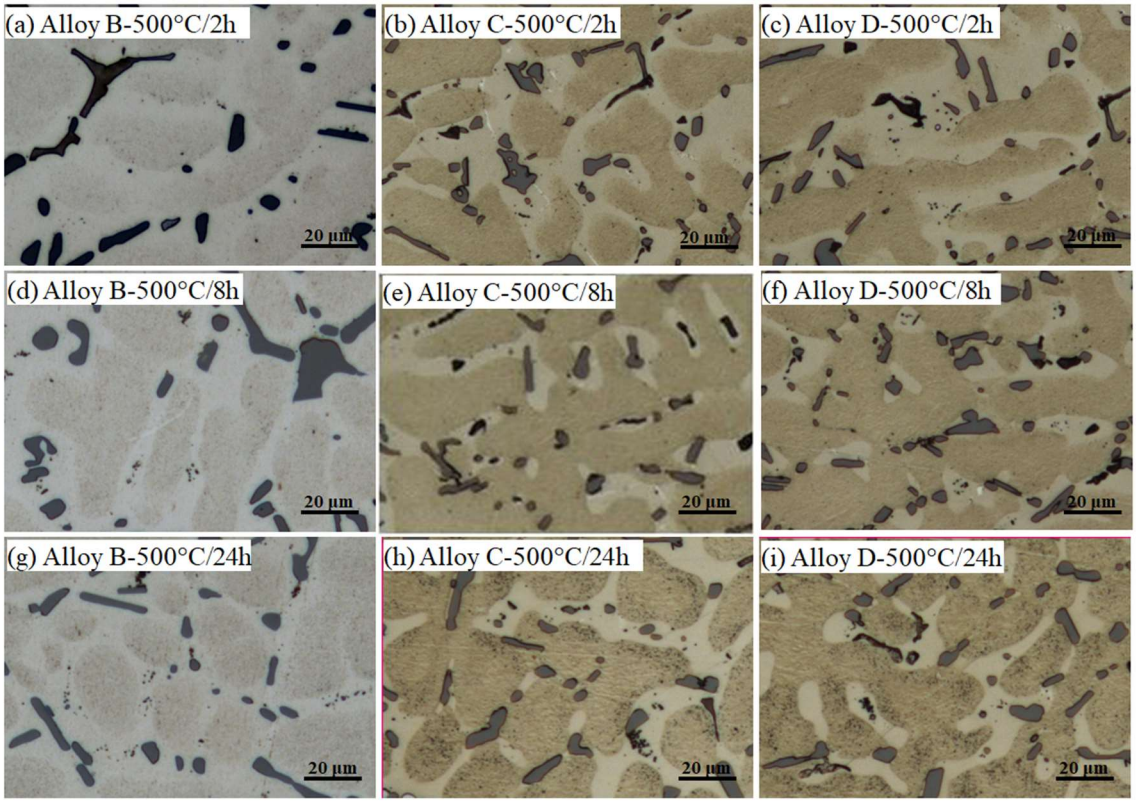

Fig. 3 Evolution of dispersoids in Alloys B, C and D at 500 °C (obtained in OM)

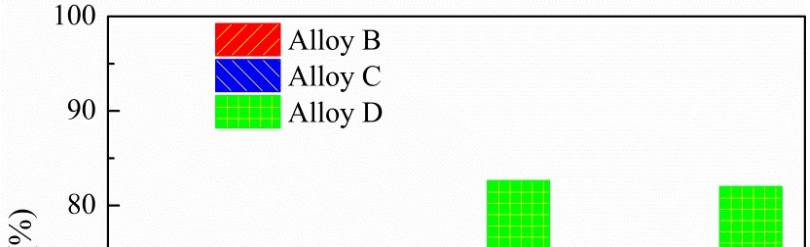

Fig.4 Area percentage of the dispersoid zone as a function of holding time at 500 °C

To investigate the dispersoids in detail, TEM was employed under selected conditions at 500°C and shown in Fig. 5. Figs. 5a–c shows the distributions of dispersoids in Alloy D treated at 500°C for 2 h, 8 h, and 24 h, respectively. It can be observed that the sizes of the dispersoids were similar after 2 h and 8 h but the number density sharply increased with time (Fig. 5b). After 24 h (Fig. 5c), the dispersoids grew bigger while the number density decreased, indicating the coarsening of the dispersoids during prolonged holding. The optimal heat treatment condition for the precipitation of dispersoids was determined to be 500°C/8h based on their characteristics. Fig. 5d and 5e show the dispersoids after treatment at 500°C/8h in Alloys B and C, respectively. The dispersoids were much bigger and the number density was lower in Alloy B than those in Alloy C, confirming the more positive effect of Mo than that of Mn on dispersoid formation. This can be attributed to the lower diffusion rate of Mo than Mn, causing the lower growth rate of dispersoids [18, 19]. Therefore, the dispersoids in Alloy C were much smaller than those in Alloy B. In addition, the TEM-EDS results of the dispersoids in the three alloys, presented in Figs. 5f–h, show that the dispersoids contain Fe, Mn, and Si in Alloy B, Fe, Mo, and Si in Alloy C, and Fe, Mn, Mo, and Si in Alloy D, respectively. Despite slight differences between the dispersoid chemistries resulting from the addition of Mn and Mo, all the dispersoids are considered to be α-AlFeSi type of dispersoids, in which the Mn and Mo solutes can replace some Fe solutes, according to the literature [11, 13]. Therefore, they are indiscriminately named as α-dispersoids in the present study, which is reported to have the crystal structure of body-centered cubic (a=1.256 nm) [6, 8, 13]. It was apparent that the number density of the α-dispersoids in Alloys B and C was much lower than that in Alloy D (Fig. 5), which can be attributed to the combined additions of Mn and Mo in the latter. As proposed by Farkoosh

et al. [15], Mo segregates in the Al dendrite core, while Mn segregates in the interdendritic region owing to the opposite portioning of the Mo and Mn solute atoms during solidification. Therefore, the combined additions of Mn and Mo favorably contribute to a more uniform distribution of α-dispersoids as well as the significantly increased number density of dispersoids.

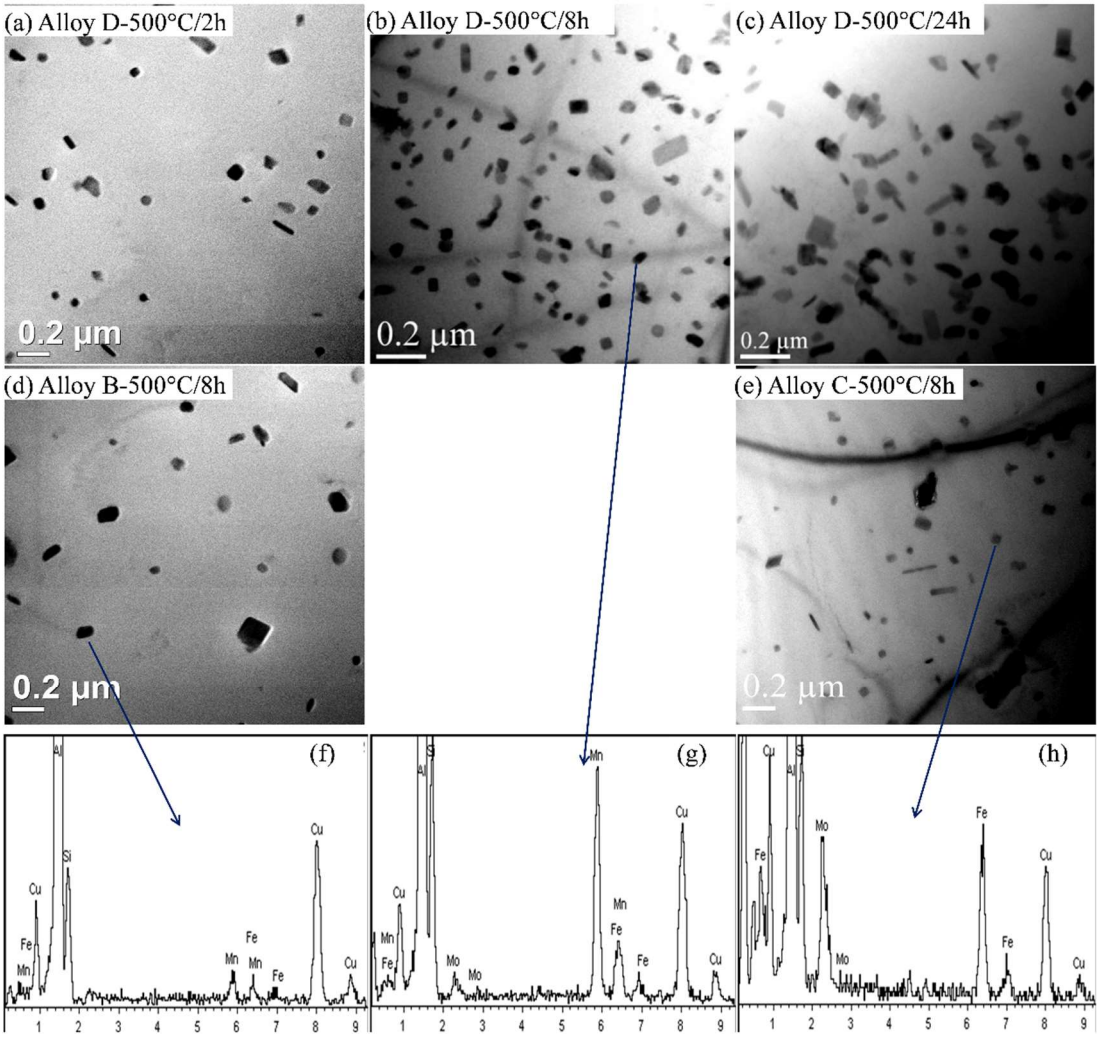

Fig. 5 TEM bright filed images showing dispersoid evolution in the three alloys and their corresponding TEM-EDS analysis results

3.3 Impact of dispersoids on mechanical properties

As shown in Figs. 3–5, the dispersoids can quickly precipitate at 500°C and reach the optimum precipitation after 500°C/8h. To determine the impact of the dispersoids on the mechanical properties at RT, YS was measured under two conditions: one is directly after the solution treatment at 500°C, labeled as "SHT", and the other one is under the "T6" condition where the aging process (155°C/5h) was further performed after solution treatment. The evolutions of YS of the experimental alloys are shown in Fig. 6.

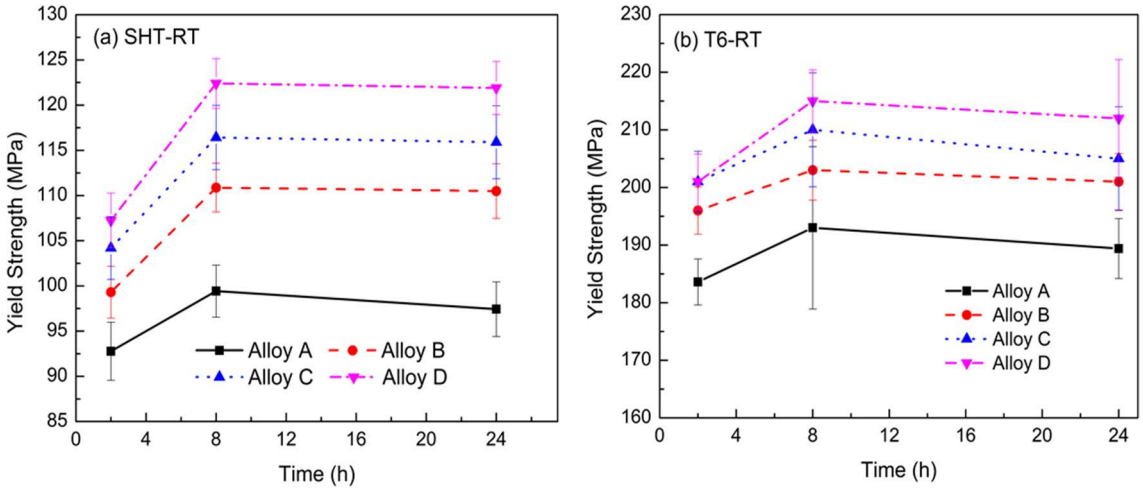

Fig.6 Evolution of YS at RT under SHT and T6 of experimental alloys

As shown in Fig. 6a, the YS under the SHT condition first increased from 2 h to 8 h and then became stable or slightly decreased after 24 h in the case of all four alloys. The increase in the YS of Alloy A from 2 h to 8 h can be attributed to the solid solution strengthening due to the gradual dissolution of Al_2Cu intermetallics into the Al matrix during the solution treatment. As the contribution of the solid solution strengthening should be the same across the four alloys owing to their similar Cu contents, the improvement in YS in the order, Alloy A < Alloy B < Alloy C < Alloy D, for a given holding time can be principally attributed to the formation of dispersoids. Following treatment at 500°C/2h, the differences between the YS values of the alloys were small due to the small number of dispersoids precipitated (Figs. 3 and 5), which were 6.5 MPa, 11.4 MPa, and 14.6 MPa between Alloys B, C, and D, respectively, when compared with that of Alloy A. After 500°C/8h, the differences increased to 11.4 MPa, 17.2 MPa, and 22.2 MPa, respectively, owing to the increasing number of dispersoids under the condition of peak precipitation in the case of Alloys B, C, and D, respectively, when compared with that of Alloy A (Fig. 5).

Under the T6 condition (Fig. 6b), YS is significantly higher than that under the SHT condition at the same time of solution treatment due to the precipitation hardening during aging. As shown in Fig. 7a-b, highly dense nanoscale precipitates were formed under the T6 condition, which are confirmed as θ"-Al_2Cu by the selected area diffraction pattern (SADP) [20-22], leading to the much higher YS. On the other hand, the evolutions of YS with time under both SHT and T6 conditions were similar that it increased from 2 h to 8 h and became stable thereafter until 24 h. As the Al-Si-Cu 319 cast alloys were heat-treatable and the four alloys in this study had the same Cu content, a similar contribution toward precipitation strengthening from θ"-Al_2Cu was expected in all four specimens, which was also confirmed by the similar precipitation behavior of θ"-Al_2Cu after T6 in Alloys A and D, as shown in Figs. 7a–b. However, remarkable higher YS were observed in Alloys B, C, and D than those in Alloy A, and the differences increased with solution time until to 8 h.

For instance, when compared with that of Alloy A, the YS of Alloy D at a holding time of 8 h increased by 23 MPa under T6 (215 MPa vs. 192 MPa). It is evident that the increasing improvement on YS in the order, Alloy A < Alloy B < Alloy C < Alloy D, was attributed to the presence of different numbers of dispersoids in the Al matrix. The slight decrease in YS after treatment at 500°C/24h was most likely owing to the coarsening of dispersoids (Fig. 5).

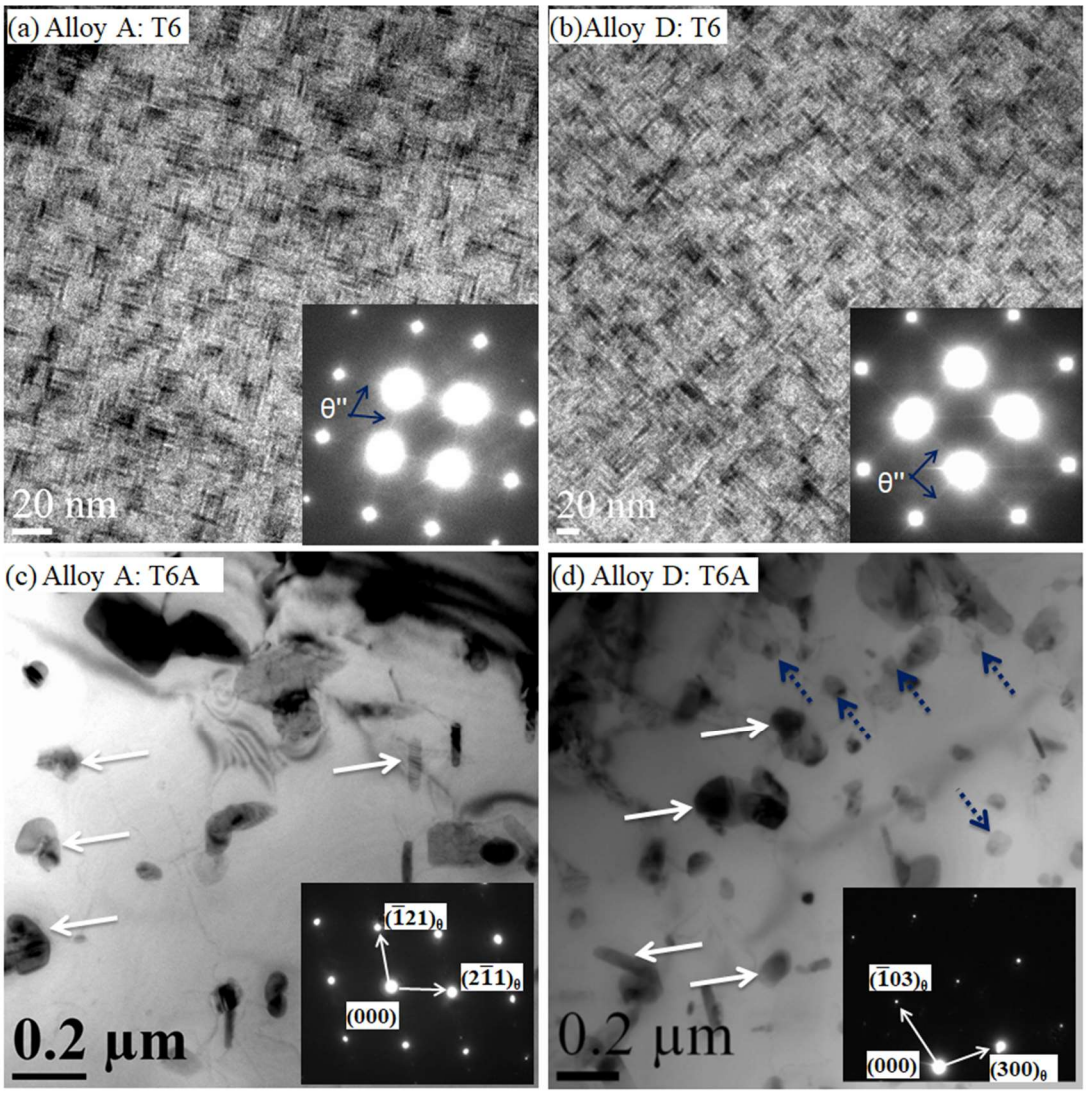

Fig. 7 TEM micrographs of Alloys A and D under T6 and T6A conditions: a) and b) θ"-Al_2Cu precipitates in the matrix, confirming with the inserts of SADP; c) θ-Al_2Cu in the matrix and d) co-existed θ-Al_2Cu (white arrows) and α-dispersoids (blue arrows) in the matrix. The θ-Al_2Cu was confirmed by the inserts of SADP in c) and d).

From the distribution of dispersoids in Figs. 3–5, the area percentage and number density of dispersoids reach the maximum at 500°C/8h, indicating that the most of supersaturated Mn atoms has been precipitated out as dispersoids. Therefore, it was

proposed that fine dispersoids could fully precipitate at 500°C/8h, resulting in a remarkable improvement in YS at RT under both SHT and T6 conditions, as shown in Fig. 6. Therefore, the YS at 300°C was further measured after T6 aging (500°C/8h + 155°C/5h) to simulate the conditions of industrial application. The YS at 300°C was measured directly after T6 (designated as "T6-ET"), while an annealing process at 300°C for 100 h was applied to the T6 samples to stabilize their microstructures before the YS measurements at 300°C (designated as "T6A-ET"). The evolution of YS at ET in the alloys is shown in Fig. 8.

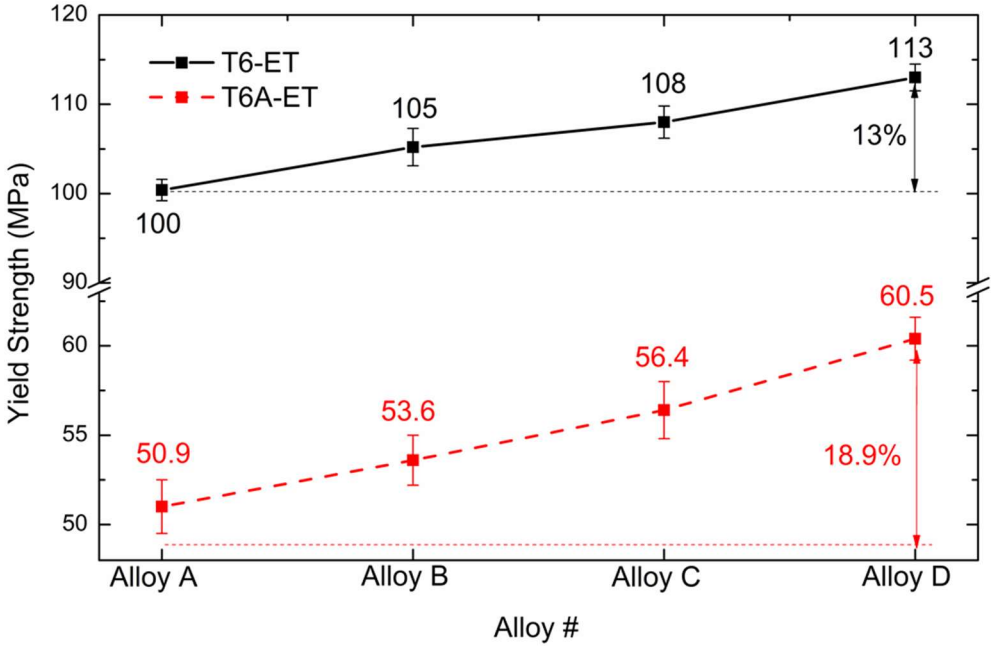

Fig. 8 Evolution of YS at ET of experimental alloys tested at 300ºC

As shown in Fig. 8, YS increased in the order Alloy A < Alloy B < Alloy C < Alloy D and reached the highest value in Alloy D under both the T6-ET and T6A-ET conditions. For instance, the YS at ET increased from 100 MPa to 113 MPa under the T6-ET condition (Fig. 8a) and from 50.9 MPa to 60.5 MPa under the T6A-ET condition (Fig. 8b) from Alloy A to Alloy D, exhibiting improvements on the YS at ET of 13 MPa (13%) and 9.6 MPa (18.9%), respectively. On the other hand, the YS under T6A-ET were always lower than those under T6-ET, which can be explained by the coarsening of the Al_2Cu precipitates during annealing (300°C/100h). As shown in Figs. 7c–d and indicated by white arrows, the Al_2Cu precipitates has transformed from the coherent θ" (T6) to the incoherent equilibrium θ phase (T6A), confirmed by SADP in the inserts of Fig. 7c-d [20-22]. Compared with those of the coherent θ"-Al_2Cu, the number density of the equilibrium θ-Al_2Cu phase had greatly decreased and size had sharply increased. Therefore, the YS was greatly decreased after T6A. However, a number of α-dispersoids were still present in Alloy D with a size range of 70-100 nm (Fig. 7d, blue arrows) and they provided an additional strengthening effect at ET, resulting in the enhanced mechanical properties at ET of Alloys B, C, and D,

which contained α-dispersoids.

As shown in Figs. 6 and 8, the YS at both RT and ET were remarkably improved in the alloys containing α-dispersoids under all tested conditions (SHT-RT, T6-RT, T6-ET, and T6A-ET). It was also observed from the YS values in Figs. 6 and 8 that the precipitation strengthening of the θ"-Al_2Cu precipitates under the T6 condition was the primary strengthening mechanism at both RT and ET. Due to the relatively low number density and relatively large size of the dispersoids when compared with those of the θ"-Al_2Cu precipitates, the presence of the dispersoids can provide a complementary strengthening effect. However, with the presence of and coarsening of θ-Al_2Cu precipitates for the T6A condition (Figs. 7c–d), the significant contribution of the dispersoids to strength became particularly obvious at ET (T6A-ET). In addition, the improvement in YS at both RT (Fig. 6) and ET (Fig. 8) from the individual addition of Mo (Alloy C) was higher than those obtained from the individual addition of Mn (Alloy B), yet the YS in both the cases were still lower than that of Alloy D, which confirmed the strongest strengthening effect arising from the combined additions of Mn and Mo.

3.4 Influence of dispersoids on creep resistance at ET

Creep resistance, which is considered one of the most important criteria for ET applications, was evaluated at 300°C under the compression mode in this study. To simulate the service condition at ET as well as to stabilize the microstructure, all the samples for the creep tests were solution-treated at 500°C/8h, then aged at 155°C/5h, and subsequently annealed at 300°C/100h (T6A). The typical creep curves of all four alloys under a constant load of 30 MPa are shown in Fig. 9. A similar creep behavior can be observed for all four experimental alloys that the creep strain increased rapidly during the first few hours in the initial stage, while the increase of creep strain moved into a quasi-steady stage. However, large differences were observed between the four alloys in terms of the maximum strain. As shown in Fig. 9, the maximum strain after 96 h had already reached 0.17 in the case of Alloy A, while it was only 0.04 in Alloy B, 0.015 in Alloy C, and even 0.006 in Alloy D, confirming the great improvement in creep resistance from the additions of Mn and Mo.

According to the literature [23, 24], the "minimum creep rate ($\dot{\varepsilon}_m$)" is calculated as the slope of the creep curve in the quasi-steady stage (see Fig. 9) since the creep deformation during this stage is becoming stable or quasi-stable due to the balance between working hardening and thermal softening. The measured maximum strain and the calculated minimum creep rate are summarized in Table 2. The measured maximum strain and the calculated minimum creep rate are summarized in Table 2. It can be found that the value of the minimum creep rate $\dot{\varepsilon}_m$ significantly decreased with increase in Mn and Mo levels. As shown in Table 2, $\dot{\varepsilon}_m$ was 5.5E-07 s^{-1} for Alloy A but it decreased to 1.0E-07 s^{-1} for Alloy B, 3.1E-08 s^{-1} for Alloy C, and further to 1.1E-08 s^{-1} for Alloy D, which was 50 times lower than that of Alloy A. In addition, it can also be found that Alloy C had lower maximum strain and minimum creep rate than those of Alloy B, confirming the

enhancement of creep resistance from the individual addition of Mo than that of Mn.

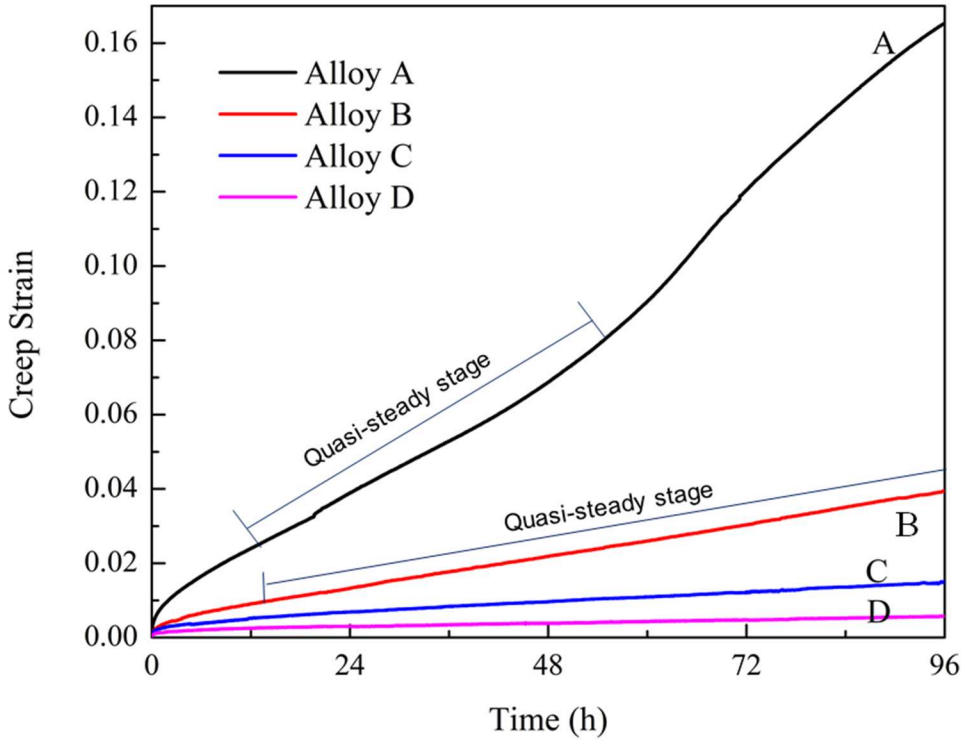

Fig. 9 Typical creep curves after T6A under a constant load of 30MPa tested at 300°C (Quasi-steady stage is indicated for Alloys A and B as example)

Table 2 The total stain and $\dot{\varepsilon}_m$ after T6A under a constant load of 30 MPa

Alloys	A	B	C	D
Total Strain	0.17	0.040	0.015	0.0057
Minimum creep rate (s^{-1})	5.5E-07	1.0E-07	3.1E-08	1.1E-08

To better understand the effects of dispersoids on the ET creep properties, additional creep tests were performed under different loads (25 MPa, 30 MPa, 35 MPa, and 40 MPa) to obtain the threshold stress (σ_{th}) and true stress exponent (n). Fig.10 shows the minimum creep rate as a function of applied load at 300°C. It can be seen that Alloy D showed the highest creep resistance, followed by Alloys C and B, and Alloy A displayed the lowest creep resistance. The threshold stress σ_{th} was calculated as the stress at a creep rate of 10^{-10} s^{-1} by extrapolating the linear-fitted double logarithmic curves of minimum creep rate vs. applied stress σ (dotted lines in Fig. 10). After determining σ_{th}, the true stress exponent n can be determined as the slope of the double logarithmic curve of $\dot{\varepsilon}_m$ vs. (σ-σ_{th}), according to the following equation [10]:

$$\dot{\varepsilon}_m = A' \left(\frac{\sigma-\sigma_{th}}{G}\right)^n \exp\left(-\frac{Q}{RT}\right), \qquad \text{Eq. 1}$$

where $\dot{\varepsilon}_m$ is the minimum creep rate, σ is the applied load, σ_{th} is the calculated threshold

stress, Q is the activation energy, G is the shear modulus, n is the true stress exponent, A′ is a constant, R is the universal gas constant, and T is the absolute temperature. The values of σ_{th} and n are listed in Table 3.

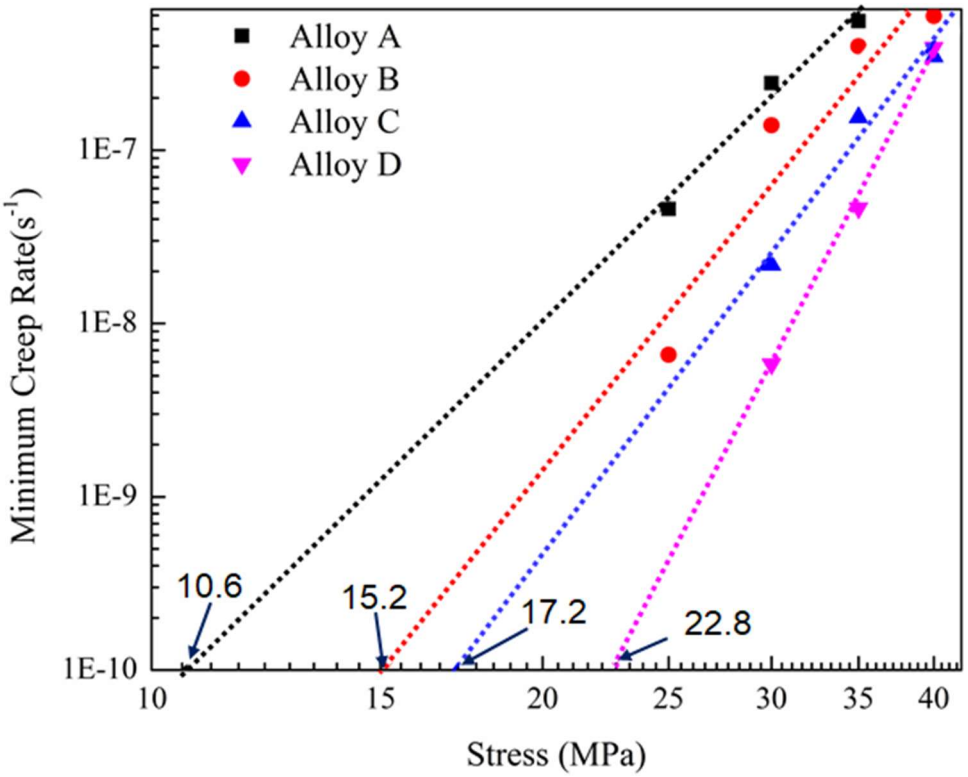

Fig. 10 Logarithmic plots of minimum creep rate $\dot{\varepsilon}_m$ vs. applied stress σ for experimental alloys tested at 300°C

Table 3 Creep properties of the experimental alloys

Creep property	Alloys			
	Alloy A	Alloy B	Alloy C	Alloy D
Threshold Stress (MPa)	10.6	15.2	17.2	22.8
True Stress Exponent(n_t)	3.93	3.83	3.84	3.37

As shown in Table 3, the calculated true stress exponent n of the four alloys were approximately 3–4, indicating that creep deformation was principally controlled by the movement of dislocations in the studied alloys [25-27]. Consequently, the factors that can affect the movement of dislocations are the solid solution atoms, precipitates, and dispersoids. As discussed in Sections 3.2 and 3.3, the solid solution level and precipitates should be similar in the four alloys after T6A; thus, the greatest contributors toward creep resistance are the size and number density of dispersoids.

The threshold stress, σ_{th}, is generally considered to be the stress required to detach a

dislocation from an obstacle or the additional stress required to climb over an obstacle [24, 28]. As shown in Table 3, the value of σ_{th} increased from 10.6 MPa in Alloy A to 15.2 in Alloy B, 17.2 in Alloy C, and further to 22.8 MPa in Alloy D. It is also reported that an increase of 3 MPa in σ_{th} is approximately equivalent to an order of magnitude decrease in the minimum creep rate [14]. In this study, an increase of 12.8 MPa in σ_{th} from Alloy A to Alloy D was achieved, while the minimum creep rate decreased by a factor of 50. The near doubling of σ_{th} from Alloy A to D can principally be attributed to the increasing number density of dispersoids, further confirming the strong effect of dispersoids on creep resistance as well as on the improvements in mechanical properties (YS). Furthermore, the reduction in DFZs, where dislocations can move freely at low stress, owing to the increase in the dispersoid zones from Alloy A to Alloy D with the additions of Mn and Mo (Fig. 4), favors an effective dislocation pinning, thus contributing to the increase in σ_{th} [29].

3.5 Long-term thermal stability of ET properties

The long-term thermal stability of mechanical properties during service is another important consideration for the components operating at ET. In the present study, a thermal exposure at 300°C for up to 1000 h was performed after T6 to evaluate the long-term thermal stability. Fig. 11 displays the evolution of YS of the four alloys during the prolonged thermal exposure. Apparently, all four alloys experienced decreases in YS with time due to the continuous coarsening of Al_2Cu precipitates. However, the decline rate varied across alloys and was lower in the alloys with added Mn and Mo. For instance, the YS of Alloy A dropped from 51 MPa after 100 h to 35.4 MPa after 1000 h, which was a 30% decrease. On the other hand, the YS of Alloy D decreased from 60.4 MPa after 100 h to 54.3 MPa after 1000 h, which was only a 10.1% decrease, and this was owing to the presence of a large number of dispersoids, causing Alloy D to exhibit the best thermal stability. The declines in the YS of Alloys B and C (18.9% in Alloy B and 16.1% in Alloy C) were between those of Alloys A and D, showing different degrees of improvement in thermal stability.

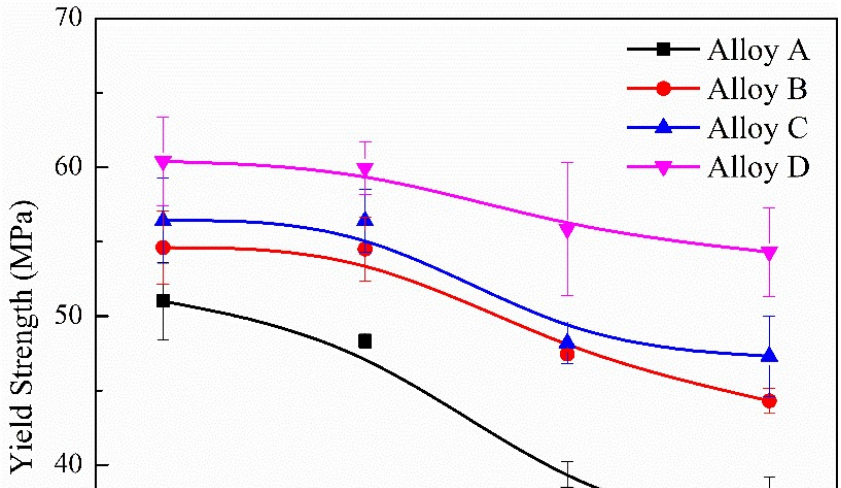

Fig. 11 Evolution of YS at 300 °C of alloys after thermal exposure at 300 °C

Creep tests were additionally performed after the long-term thermal exposure at 300°C for 1000 h after T6. Fig. 12a-b shows the typical creep curves of Alloys A and D after thermal exposure for 100 h and 1000 h. It can be observed that the creep strains are much higher in Alloy A than Alloy D. Meanwhile, the creep strains in both alloys were increasing with the time but the increasing rate was much lower in Alloy D than that in Alloy A. The maximum strain and minimum creep rate of four experimental alloys after 100 h and 1000 h are summarized in Fig. 12c-d. The maximum creep strain and minimum creep rate of all the four alloys increased after 1000 h when compared with those after 100 h, which could be attributed to the coarsening of Al_2Cu precipitates [30]. Similar to the evolution of YS during thermal exposure, the extent of increase in creep resistance also varied across alloys. For instance, in Alloy A, the maximum creep strain increased from 0.17 to 0.25, which was a 47% increase, while the minimum creep rate increased from 5.5E-07 to 6.8E-07. Alloys B and C exhibited moderate increases in both the maximum strain and the minimum creep rate, indicating an improved thermal stability over that of alloy A. On the other hand, the maximum creep strain and minimum creep rate of Alloy D remained almost unchanged after 1000 h of prolonged exposure at 300°C, showing the best long-term thermal stability.

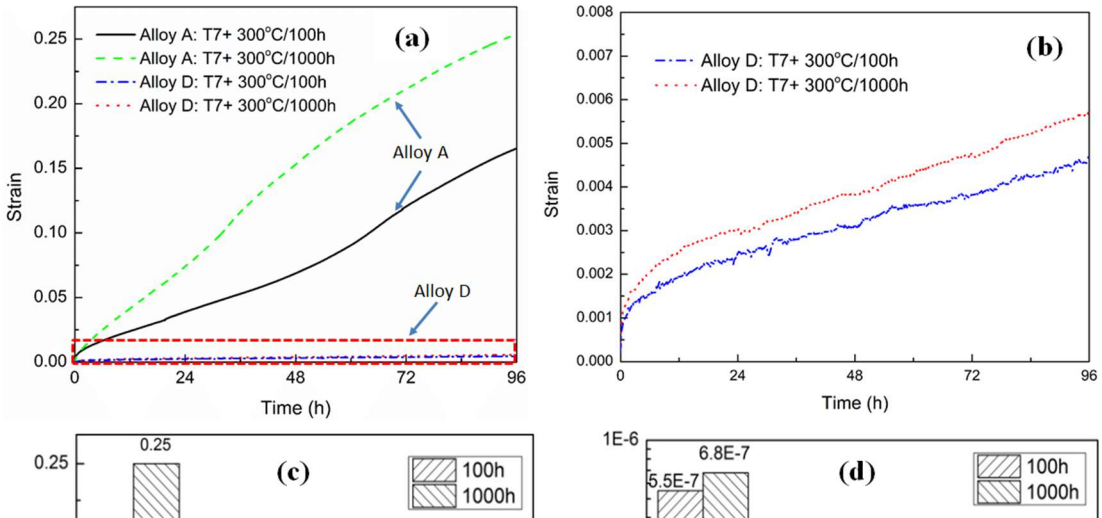

Fig. 12 Typical creep curves of Alloys A and D after thermal exposure at 300 °C for 100 h (a) and 1000 h (enlarged view, b); and the evolution of the total strain (c) and the minimum creep rate (d) of experimental alloys during the thermal exposure.

Fig. 13 shows the TEM micrographs of the Al_2Cu precipitates and α-dispersoids in Alloys A and D after thermal exposure at 300°C for 1000 h. Compared with the microstructures at 300°C for 100 h (TEM images in Figs. 7c–d), the equilibrium non-coherent θ-Al_2Cu phases in both the alloys (indicated by red arrows) continued to coarsen. Their sizes can reach approximately 300–600 nm, and thus the interparticle space between θ-Al_2Cu particles increased considerably (350-400 nm after T6+300°C/1000h in Fig. 13a vs. 150-200 nm after T6+300°C/1000h in Fig. 7c). The coarsening behavior of Al_2Cu precipitates in an Al-Cu-Mg alloy during thermal holding at 250°C was investigated in [31] and a similarly coarsened θ-Al_2Cu microstructure was obtained after 2000 h. On the other hand, α-dispersoids are thermally stable in the temperature range 300–350°C [8, 11]. Fig.13b clearly demonstrates that the size and number density of α-dispersoids in Alloy D remained unchanged even after 1000 h compared with those after 100 h (Fig. 7d, blue arrows). Consequently, the dispersoid strengthening became the major strengthening mechanism after the main strengthening phase i.e., Al_2Cu precipitates, coarsened at ET.

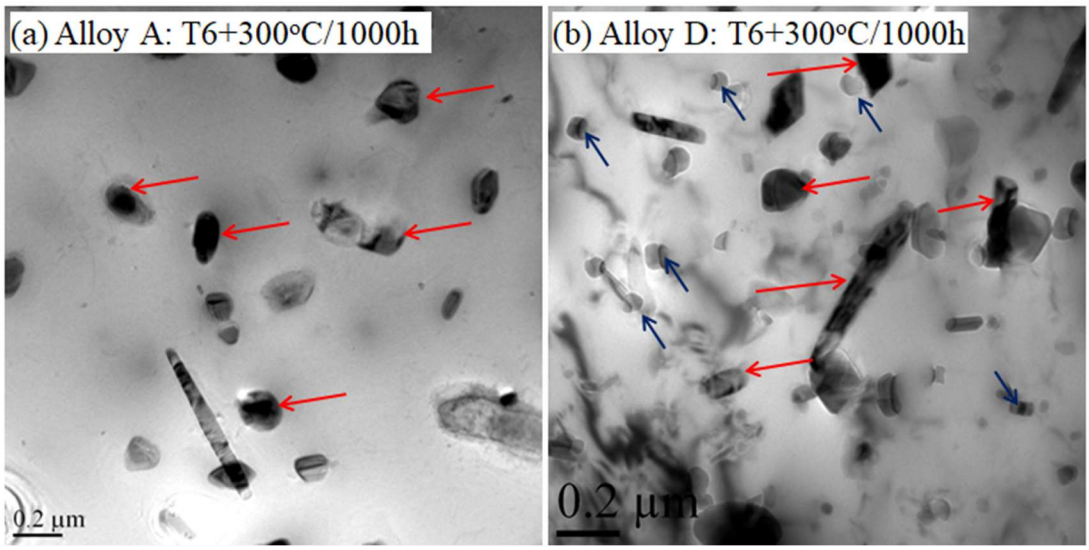

Fig. 13 TEM bright field images showing Al_2Cu precipitates and α-dispersoids in Alloys A and D during thermal exposure at 300 ºC for 1000 h

Although the Al_2Cu precipitates in all the alloys coarsened during prolonged thermal exposure, the decline rate of YS and creep resistance (Figs. 11 and 12) were considerably decreased in the order, Alloy B > Alloy C > Alloy D, owing to the increasing presence of thermally stable dispersoids. It was also interesting to note that the dispersoids were more efficient in increasing creep resistance than in increasing YS. For instance, when compared with that of the base alloy (Alloy A), the minimum creep rate of Alloy D, which had the largest number of dispersoids in the Al matrix, was reduced by approximately 50 times after treatment at 300ºC/100h and remained almost unchanged at those low levels even after prolonged exposure for 1000 h at the same temperature. On the other hand, the increment in YS from the base alloy (Alloy A) to Alloy D was 10 MPa after 300ºC/100h, representing an improvement of approximately 20%; however, after prolonged exposure for 1000 h, the YS of Alloy D slightly decreased. It is known that YS at ET can still be described by the Orowan dislocation bypass model [32]. When the particles are not shareable, the smaller the particle size, the larger is the contribution to improvement in YS. However, the creep deformation at ET is mainly controlled by dislocation climb and detachment [33]. Although the exact nature of the dislocation activities under creep condition and the resultant creep properties (the minimum creep rate and threshold stress) are unknown, it appears that a reasonably large size of partially coherent particles (still in the nano-scale dispersoids, between 50 nm to 100 nm in this work) could be favorable to a significant increase in creep resistance.

4. Conclusions

1) The additions of both Mn and Mo can promote the precipitation of α-dispersoids in Al-Si-Cu 319 cast alloys. The individual addition of Mo had a stronger effect than that of Mn, but the combined addition of the two elements showed the best effect in the Mn and Mo range studied.
2) The α-dispersoids started to form at 450°C and the optimum condition for dispersoid precipitation with the largest number density and finest size was attained after treatment at 500°C/8h.
3) The α-dispersoids can provide a complementary strengthening effect on the mechanical properties, resulting in remarkable improvements in YS at both room and elevated temperatures. An improvement of 19% in YS at 300°C was achieved in the

T6 samples after stabilization at 300°C for 100 h by the combined addition of Mn and Mo.

4) The creep resistance at 300°C was greatly improved with the additions of Mn and Mo. Compared with the base alloy free of Mn and Mo, the minimum creep rate decreased from 5.5E-07 s^{-1} to 1.1E-08 s^{-1}, while the threshold stress increased from 10.6 MPa to 22.8 MPa in the alloy with both Mn and Mo added.
5) During prolonged thermal exposure at 300°C for up to 1000 h, the main strengthening phase (Al_2Cu precipitates) inevitably coarsened while the α-dispersoids remained stable. The alloy with both Mn and Mo added exhibited the lowest rate of decline in YS and unchanged minimum creep rate, showing the superior thermal stability of Al-Si-Cu 319 alloys at elevated temperature due to the presence of a sufficient number of dispersoids.

Acknowledgements

The authors would like to acknowledge the financial support from the Natural Sciences and Engineering Research Council of Canada (NSERC) and Rio Tinto Aluminum, through the NSERC Industry Research Chair in Metallurgy of Aluminum Transformation at the University of Quebec at Chicoutimi.

References

[1] M. Javidani, D. Larouche, Application of cast Al–Si alloys in internal combustion engine components, Int. Mater. Rev. 59(3) (2014) 132-158.
[2] S. Alkahtani, Mechanical performance of heat treated 319 alloys as a function of alloying and aging parameters, Mater. Des. 41 (2012) 358-369.
[3] A. Lombardi, C. Ravindran, R. MacKay, Optimization of the solution heat treatment process to improve mechanical properties of 319 Al alloy engine blocks using the billet casting method, Mater. Sci. Eng., A 633 (2015) 125-135.
[4] J.G. Kaufman, Properties of aluminum alloys : tensile, creep, and fatigue data at high and low temperatures, ASM International ; Aluminum Association, Materials Park, Ohio; Washington, D.C., 1999.
[5] Y.J. Li, L. Arnberg, Quantitative study on the precipitation behavior of dispersoids in DC-cast AA3003 alloy during heating and homogenization, Acta Mater. 51(12) (2003) 3415-3428.
[6] Y.J. Li, A.M.F. Muggerud, A. Olsen, T. Furu, Precipitation of partially coherent α-Al(Mn,Fe)Si dispersoids and their strengthening effect in AA 3003 alloy, Acta Mater. 60(3) (2012) 1004-1014.
[7] K. Liu, X.-G. Chen, Evolution of microstructure and elevated-temperature properties with Mn addition in Al-Mn-Mg alloys, J. Mater. Res. 32(13) (2017) 2585-2593.
[8] K. Liu, X.G. Chen, Development of Al–Mn–Mg 3004 alloy for applications at elevated temperature via dispersoid strengthening, Mater. Des. 84 (2015) 340-350.
[9] K. Liu, X.G. Chen, Evolution of Intermetallics, Dispersoids, and Elevated Temperature Properties at Various Fe Contents in Al-Mn-Mg 3004 Alloys, Metall. Mater. Trans. B 47B (2015) 3291-3300.

[10] K. Liu, H. Ma, X.G. Chen, Improving the Elevated-Temperature Properties by Two-Step Heat Treatments in Al-Mn-Mg 3004 Alloys, Metall. Mater. Trans. B 49(4) (2018) 1588-1596.
[11] K. Liu, H. Ma, X.G. Chen, Enhanced elevated-temperature properties via Mo addition in Al-Mn-Mg 3004 alloy, J. Alloys Compd. 694 (2017) 354-365.
[12] K. Liu, X.G. Chen, Influence of heat treatment and its sequence on elevated-temperature properties of Al-Mn-Mg 3004 alloy, Mater. Sci. Eng. A 697 (2017) 141-148.
[13] A.R. Farkoosh, X.G. Chen, M. Pekguleryuz, Interaction between molybdenum and manganese to form effective dispersoids in an Al–Si–Cu–Mg alloy and their influence on creep resistance, Mater. Sci. Eng., A 627 (2015) 127-138.
[14] A.R. Farkoosh, X. Grant Chen, M. Pekguleryuz, Dispersoid strengthening of a high temperature Al–Si–Cu–Mg alloy via Mo addition, Mater. Sci. Eng., A 620 (2014) 181-189.
[15] S. Seifeddine, S. Johansson, I.L. Svensson, The influence of cooling rate and manganese content on the β-Al5FeSi phase formation and mechanical properties of Al–Si-based alloys, Mater. Sci. Eng. A 490(1) (2008) 385-390.
[16] S.G. Shabestari, The effect of iron and manganese on the formation of intermetallic compounds in aluminum–silicon alloys, Mater. Sci. Eng. A 383(2) (2004) 289-298.
[17] L. Jin, K. Liu, X.G. Chen, Evolution of Fe-Rich Intermetallics in Al-Si-Cu 319 Cast Alloy with Various Fe, Mo, and Mn Contents, Metall. Mater. Trans. B 50(4) (2019) 1896-1907.
[18] K.E. Knipling, D.C. Dunand, D.N. Seidman, Criteria for developing castable, creep-resistant aluminum-based alloys - A review, Z. METALLKD 97(3) (2006) 246-265.
[19] C.J. Kuehmann, P.W. Voorhees, Ostwald ripening in ternary alloys, Metall. Mater. Trans. A 27(4) (1996) 937-943.
[20] A. Wiengmoon, J.T.H. Pearce, T. Chairuangsri, S. Isoda, H. Saito, H. Kurata, HRTEM and HAADF-STEM of precipitates at peak ageing of cast A319 aluminium alloy, Micron 45 (2013) 32-36.
[21] E.M. Elgallad, P. Shen, Z. Zhang, X.G. Chen, Effects of heat treatment on the microstructure and mechanical properties of AA2618 DC cast alloy, Mater. Des. 61 (2014) 133-140.
[22] A. Biswas, D.J. Siegel, C. Wolverton, D.N. Seidman, Precipitates in Al–Cu alloys revisited: Atom-probe tomographic experiments and first-principles calculations of compositional evolution and interfacial segregation, Acta Mater. 59(15) (2011) 6187-6204.
[23] B.G. Kim, J.L. Rempe, D.L. Knudson, K.G. Condie, B.H. Sencer, In-Situ Creep Testing Capability for the Advanced Test Reactor, Nucl. Technol. 179(3) (2012) 417-428.
[24] L. Pan, K. Liu, F. Breton, X.-G. Chen, Effect of Fe on Microstructure and Properties of 8xxx Aluminum Conductor Alloys, J. Mater. Eng. Perform. 25(12) (2016) 5201-5208.
[25] H.R. Erfanian-Naziftoosi, E.J. Rincón, H.F. López, Creep Properties of the As-Cast Al-A319 Alloy: T4 and T7 Heat Treatment Effects, Metall. Mater. Trans. A 47(8) (2016) 4258-4267.
[26] L. Pan, F.A. Mirza, K. Liu, X.G. Chen, Effect of Fe-rich particles and solutes on the creep behaviour of 8xxx alloys, Mater. Sci. Technol. 33(9) (2017) 1130-1137.
[27] L. Shi, D.O. Northwood, Recent progress in the modeling of high-temperature creep and its application to alloy development, J. Mater. Eng. Perform. 4(2) (1995) 196.
[28] J. Rösler, E. Arzt, The kinetics of dislocation climb over hard particles—I. Climb without attractive particle-dislocation interaction, Acta Metall. 36(4) (1988) 1043-1051.

[29] F. Carreño, O.A. Ruano, Threshold stresses in high temperature deformation of dispersion strengthened aluminum alloys, Mater. Sci. Eng., A 214(1) (1996) 177-180.
[30] Y.H. Gao, C. Yang, J.Y. Zhang, L.F. Cao, G. Liu, J. Sun, E. Ma, Stabilizing nanoprecipitates in Al-Cu alloys for creep resistance at 300°C, Mater. Res. Lett. 7(1) (2019) 18-25.
[31] S.P. Ringer, W. Yeung, B.C. Muddle, I.J. Polmear, Precipitate stability in Al-Cu-Mg-Ag alloys aged at high temperatures, Acta Metal. Maer. 42(5) (1994) 1715-1725.
[32] D.N. Seidman, E.A. Marquis, D.C. Dunand, Precipitation strengthening at ambient and elevated temperatures of heat-treatable Al(Sc) alloys, Acta Mater. 50(16) (2002) 4021-4035.
[33] M.E. Krug, D.C. Dunand, Modeling the creep threshold stress due to climb of a dislocation in the stress field of a misfitting precipitate, Acta Mater. 59(13) (2011) 5125-5134.